Photoconductivity: A probe of defect states in carbon aerogels

Gillian A. M. Reynolds, Z. H. Wang, and M. S. Dresselhaus
Department of Physics,
Massachusetts Institute of Technology, Cambridge, Massachusetts 02139

A. W. P. Fung
Department of Electrical Engineering and Computer Science,
Massachusetts Institute of Technology, Cambridge, Massachusetts 02139

R. W. Pekala
Department of Chemistry and Materials Science, Lawrence Livermore National Laboratory,
Livermore, California 94550
(Received 9 September 1993)

The photoconductivity and dark conductivity of carbon aerogels with various heat-treatment temperatures, T_{HT}, and densities are studied. Unlike the trend for as-prepared samples, the magnitude of the photoconductivity for heat-treated ($T_{HT} > 1050\,^{\circ}C$) carbon aerogel samples decreases as the sample density and heat-treatment temperature increase. We propose a model which quantitatively explains the observed temperature dependence of the photoconductivity data. Based on this model, we attribute the observed photoconductivity to photoholes present in the system. The number of defect states and their corresponding energy decrease with increasing T_{HT} and increasing density. The decrease in the energy is attributed to a decrease in the screening effect of the defects on trapped charges. The effect of increasing the heat-treatment temperature causes the structure of the carbon aerogel to become more graphitic, especially for aerogel samples with higher mass density.

I. INTRODUCTION

Low-density microcellular materials (LDMM's) have been of interest for the past decade because of their high porosities ($> 75\%$), small cell sizes ($< 20\mu$), and distinct microstructures, making these materials of significant interest for industrial applications.[1] Traditional porous materials (e.g., foams, membranes) have generally been made with low densities at the expense of larger cell size and vice versa. Aerogels are a special type of LDMM in which all structural features (i.e., pores, particles) occur on a size scale of less than 500 Å.

On a microscopic scale, carbon aerogels are composed of covalently bonded particles, connected in a "string-of-pearls" configuration. Inside each particle ($\sim$ 120 Å diameter for the material used in this work) is an intertwined network of graphitic ribbons whose narrowest dimension is on the order of $\sim$ 25 Å. Characterization studies have been performed on carbon aerogels to better understand their mechanical, electrical, thermal, and acoustic properties.[2–4] These studies included, among others, Raman spectroscopy, magnetic susceptibility, and dc electrical resistivity measurements as a function of the carbon aerogel mass density, ρ_m. It was found[4] that the particle size and the amount of disorder inside the particles are independent of the mass density, whereas the packing ratio of particles and the conductivity are strongly dependent on the density, the conductivity increasing with increasing density, with the sharpest increase occurring at low temperatures.

To further understand the relation between the structure and the transport properties, heat-treated samples were studied.[5] Heat-treated aerogels are pyrolyzed in an inert atmosphere at temperatures $> 1050\,^{\circ}C$. It was found[5] that heat treatment tends to reduce the disorder and hence increases the conductivity of the aerogels. Magnetic susceptibility measurements[5] showed that the concentration of unpaired spins decreases with increasing heat-treatment temperature, consistent with a decrease in disorder. The unpaired spins presumably arise from defect states like dangling bonds. The large surface areas of carbon aerogels make them conducive to many defect states. The role of these defects on the conduction mechanism has not been clarified, nor has the effect of heat treatment on the transport and defect properties of carbon aerogels been fully understood.

This study investigates the defect states of carbon aerogels by probing the photoconductivity.[6] A model is introduced to explain the observed temperature dependence of the photoconductivity. We have observed a persistent photoconductivity, with decay times on the order of seconds at low temperature. The behavior is consistent with that observed by Hosoya *et al.*[7] on as-prepared carbon aerogels. Also, our data indicate that there is an increased ordering of the aerogel system with increasing heat-treatment temperature, T_{HT}, similar to the behavior observed for other disordered carbons.[8–10]

In this paper, the experimental procedures are described in Sec. II, while Sec. III discusses the experimental results for the dark conductivity and photocon-

ductivity. In Sec. IV, a model is introduced to explain the observed temperature dependence of the photoconductivity. Our conclusions are presented in Sec. V.

II. EXPERIMENTAL DETAILS

Carbon aerogels are derived from the pyrolysis of resorcinol-formaldehyde aerogels.[11,12] The latter materials are formed from the sol-gel polymerization of formaldehyde with resorcinol (1,3 dihydroxy benzene), mixed in deionized water at a 1:2 molar ratio of resorcinol/formaldehyde. Sodium carbonate is added as a base catalyst. The solution is poured into glass vials and heated at 50–95 °C to form a cross-linked gel. The resorcinol-formaldehyde gels are washed with acetone and supercritically dried from carbon dioxide (T_c=31 °C, P_c=7.4 MPa). The resultant aerogels are then pyrolyzed in a tube furnace under nitrogen flow. The [resorcinol]/[catalyst] (R/C) molar ratio is one of the parameters that controls the particle size, surface area, and degree of interconnectivity in carbon aerogels. In this study, all samples were prepared at R/C=200, resulting in a particle diameter of $\sim$ 120 Å. As-prepared carbon aerogels were pyrolyzed at 1050 °C for 4 h, while the heat-treated samples were pyrolyzed at higher temperatures for a similar time period. The mass density, ρ_m, the heat-treatment temperature, T_{HT} and room-temperature dark conductivity values for the samples studied in this paper are listed in Table I.

For the transport and photoconductivity measurements, machined samples ($\sim$ 4.5×3×3 mm^3) were mounted on a thin sheet of insulating mica which was bonded onto a copper heat sink. The heat sink was placed in a variable-temperature cryogenic optical Dewar with the sample being cooled by a flow of He gas. A four-point configuration of electrical contacts was made to the samples with silver epoxy. The temperature dependences of the dark conductivity and photoconductivity of these samples were measured in the range 5–300 K. Temperature control was maintained with a Lakeshore 93C temperature controller. A 488-nm wavelength Ar^+ laser was used as the illuminating source. Current leads were placed on the sides of the sample while voltage leads were positioned on top. For the photoconductivity measurements, the illumination time of the sample was controlled with a one-second shutter. The laser light was focused onto a 2-mm spot between the voltage contacts. Comparisons were made to as-prepared carbon aerogel samples,[7] with R/C=200, pyrolyzed at 1050 °C and with densities ranging from 0.103 g/cm^3 to 0.646 g/cm^3. More details about the photoconductivity measurements are given in Ref. 7.

III. EXPERIMENTAL RESULTS

A. Dark conductivity

The most striking effect of heat treatment on carbon aerogels (see Fig. 1) is seen in the temperature dependence of the dark conductivity, $\sigma(T)$, for heat-treated and as-prepared samples. The data are plotted in Fig. 1 as $\log_{10}\sigma$ vs T, the measurement temperature. The highest-density samples, heat-treated at 1500 and 1800 °C, show little measurement temperature dependence in the conductivity, though as-prepared high-density samples generally exhibit a stronger $\sigma(T)$ dependence,[7] similar to the behavior shown in Fig. 1 for the low-density samples. Thus, heat treatment has a very large effect on the dark conductivity of the high-density carbon aerogel samples, though most of the change in $\sigma(T)$ is realized before T_{HT} has reached 1800 °C. We note that the behavior at low T for the two low-density samples heat-treated to 1500 and 1800 °C is nearly the same.

The conductivity at constant measurement temperature is seen in Fig. 1 to increase with increasing sample density. For the low-density samples, the conductivity increases with increasing T_{HT}. The temperature dependence of $\sigma(T)$ is weak for $T > 50$ K, but $\sigma(T)$ decreases drastically in the low-temperature regime (<50 K) for all the low-density samples in Fig. 1. With increasing heat-treatment temperature T_{HT}, the temperature at which σ starts to decrease sharply is reduced slightly. As the

TABLE I. Characterization and photoconductivity parameters for carbon aerogels.

Heat-treatment temperature	1050 °C[a,b]	1500 °C	1800 °C	1050 °C[a,b]	1500 °C	1800 °C
Density (g/cm^3)	0.103	0.117	0.137	0.646	0.621	0.635
Conductivity at 300 K (S/cm)	0.74	1.02	1.60	22	42.36	65.0
R/C[c]			200			
Conductivity E_a (meV)	8.23	3.18	3.63	3.00	0.143	0.139
Photoconductivity ($\Delta\sigma$) T_{max} (K)	40.2	18.0	30.1	12.5	8.0	–
$\Delta\sigma$ activation energy E_A (meV)	3.3	2.2	2.4	2.50[d]	0.67	–
$\Delta \equiv (E_t - E_F)$ (meV)	16.8	10.3	13.7	10.6	4.31	–
B	37	120	73	–	–	–
N_t (cm^{-3})	10^{20}	3×10^{19}	10^{19}	–	–	–
p_0 (cm^{-3})	3×10^{18}	2×10^{17}	10^{17}	–	–	–

[a]As-prepared.
[b]Data obtained by application of model to as-prepared high-density sample in Ref. 7.
[c]Resorcinol/Catalyst ratio.
[d]Extrapolated value.

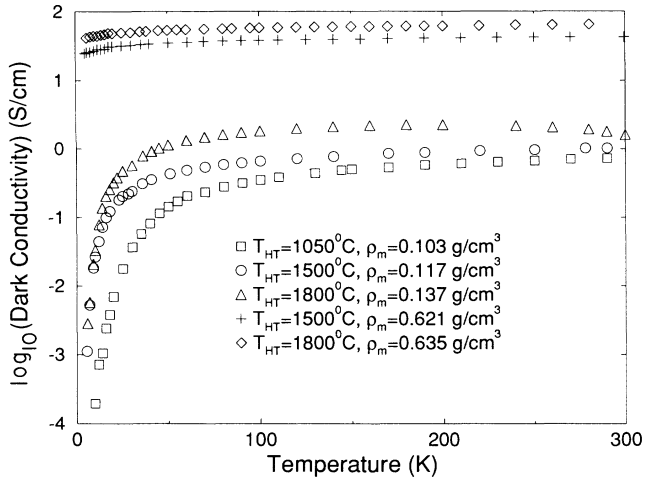

FIG. 1. Semilog plot of dark conductivities vs temperature for the carbon aerogel samples studied (see legend). For the T_{HT}=1800°C (ρ_m=0.635 g/cm^3) and T_{HT}=1500°C (ρ_m=0.621 g/cm^3) high-density samples, the temperature dependence of the dark conductivity is very weak.

density increases, the T dependence of $\sigma(T)$ becomes less pronounced and the overall room-temperature conductivity increases.

To provide a more detailed comparison of $\sigma(T)$ for the low-density samples, the data in Fig. 1 are plotted in Fig. 2 as $\log_{10}\sigma(T)$ vs $1000/T$. We can see in Fig. 2 that for all samples the data over the temperature range T <50 K exhibit a linear relation, suggesting a thermally activated conductivity, $\sigma(T) \propto \exp[-E_a/kT]$. The activation energies, E_a, thus obtained, are displayed in Table I. It can be seen that generally the activation energies decrease with increasing T_{HT} and density.

B. Photoconductivity

The photoconductivity, $\Delta\sigma$, for three low-density samples with different heat-treatment temperatures is plotted as a function of measurement temperature, T, in Fig. 3. The inset shows $\Delta\sigma$ versus T for a high-density sample (ρ_m=0.621 g/cm^3) with T_{HT}=1500 °C. The solid lines are calculated based on the model described in the next section and are compared to the experimental data points. One interesting feature in the photoconductivity data is the occurrence of a maximum in the plots of $\Delta\sigma$ versus T. The photoconductivity follows a simple activated form, $\Delta\sigma \propto \exp[-T_0/T]$ at low T and $\Delta\sigma \propto \exp[T_1/T]$ at high T. The temperature where the photoconductivity is maximum, denoted by T_{max}, occurs at approximately the same temperature where the dark conductivity falls off sharply (see Fig. 1). As T_{HT} is increased, T_{max} moves to lower temperatures, tracking the behavior of the dark conductivity. Again, the effect of density change is greater on the parameters of the model than the effect of heat treatment for the two density ranges (near 0.1 g/cm^3 and 0.6 g/cm^3) studied in this work.

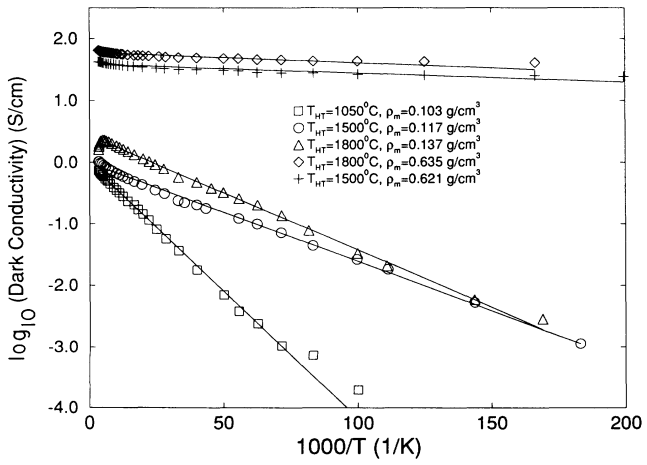

FIG. 2. Arrhenius plot of dark conductivity for as-prepared and heat-treated carbon aerogel samples. The values of the activation energies E_a for each sample are given in Table I.

Figure 3 shows that the slope of $\Delta\sigma$ versus T on the low-temperature side of T_{max} is larger than that on the high-temperature side. No photoconductivity signal could be detected for the high-density sample (ρ_m=0.635 g/cm^3) with T_{HT}=1800 ° C, although the inset to Fig. 3 for a high-density sample with T_{HT}=1500 °C and previous work[7] on a high-density as-prepared sample (ρ_m=0.646 g/cm^3) do exhibit a measurable photoconductivity. The large photoconductivity value for the high-density heat-treated sample (ρ_m = 0.621 g/cm^3, T_{HT}=1500 °C) can be understood by noting that the dark conductivity is very large for this sample, signifying a mobility greater than that for the low-density aerogels. Since $\Delta\sigma \propto \mu$, the magnitude of the photoconductivity should also scale as the mobility, conforming to our experimental data.

To further investigate the properties of the photoconductivity, Fig. 4 shows a semilog plot of $\Delta\sigma/\sigma$ versus T. All samples show a monotonic decrease in $\Delta\sigma/\sigma$ with increasing T and no maximum in $\Delta\sigma/\sigma$ is observed, in contrast to the behavior of $\Delta\sigma(T)$ itself shown in Fig. 3. With increasing T_{HT}, there is a decrease in $\Delta\sigma/\sigma$ at all temperatures for the low-density samples. The decrease in $\Delta\sigma/\sigma$ with increasing density (at T_{HT}=1500 °C) is even more pronounced. A log-log plot of photoconductivity versus laser intensity is shown in Fig. 5 for various carbon aerogel samples. The data presented in Fig. 5 were taken at 10 K. The slopes of the lines are on the order of unity. Further discussion of the observed features of the photoconductivity is presented in the next section.

IV. DISCUSSION

In order to understand the behavior of the photoconductivity of carbon aerogels, we first look at their dark conductivity. Detailed discussions on the dark conductivities for samples with various densities and heat-treatment temperatures are given elsewhere.[5,13] Previous work[4,7] has shown that the fluctuation-induced-tunneling model (FIT), given below, fits the $\sigma(T)$ data fairly well. However, recent findings[13] show that this model results in

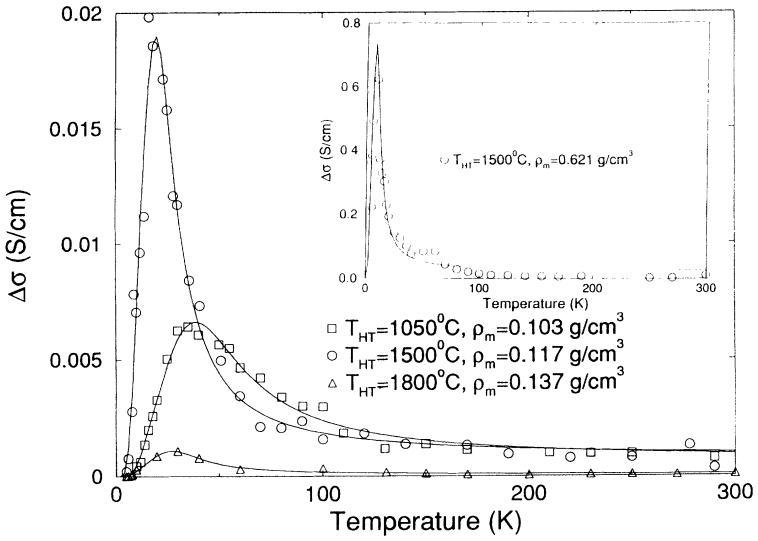

FIG. 3. Linear plot of photoconductivity vs temperature for three low-density carbon aerogel samples heat-treated to different T_{HT} values. The inset shows the same plot for a high-density sample with ρ_m=0.621 g/cm^3 and T_{HT} = 1500 ° C. Solid curves show the fit of the data points to Eq. (14).

unreasonably large effective masses for the charge carriers ($\sim$ 40 m_e for the low-density sample). Recent findings also show that variable range hopping is a more likely conduction mechanism than FIT at very low temperatures (T <10 K). Furthermore, our $\sigma(T)$ measurements, made above 4.2 K, could not possibly distinguish between the thermally activated conduction and the FIT model (given by $\sigma(T) = \sigma_0 \exp\{-[T_1/(T+T_0)]\}$) when the observed values of T_0 are less than 4 K.

The thermal activation form of the conductivity at low temperature, $\sigma(T) \propto \exp[-E_a/kT]$, suggests nearest-neighbor hopping as the dominant conduction mechanism in carbon aerogels. As we know, the aerogel system has a "string-of-pearls" morphology with graphitic ribbons within the particles. These ribbons are stacks of well-formed graphene platelets with a width of $\sim$ 25 Å as deduced from Raman scattering experiments.[4] Theoretical calculations[14,15] have shown that for a graphite sheet with finite size, there exists a band gap E_g determined by the size of the platelet (W) according to

$$E_g = \frac{21}{W} \tag{1}$$

where E_g is in electron volts and W is in Å. For a ribbon of width 25 Å, Eq. (1) suggests a band gap $E_g \sim 1$ eV, which is much larger than the experimentally measured values of E_a, which are on the order of a few meV. Thus, the temperature-dependent behavior of σ cannot be attributed to the thermal activation of charge carriers across this band gap. Hence, we attribute this thermal activation behavior to hopping between nearest-neighbor

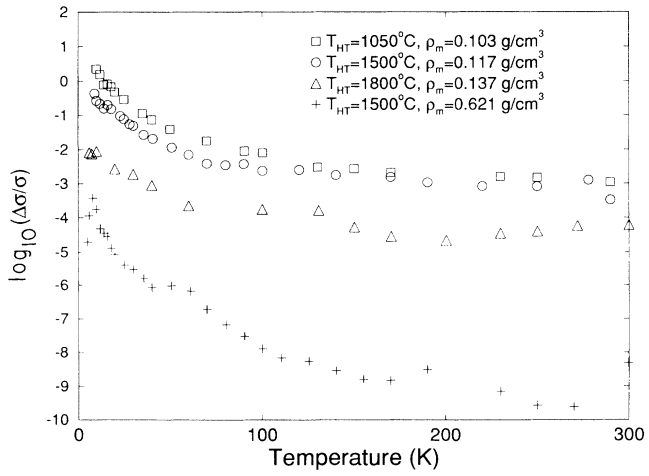

FIG. 4. Semilog plot of $\Delta\sigma/\sigma$ versus measurement temperature for carbon aerogel samples with various mass densities ρ_m and heat-treatment temperatures T_{HT}.

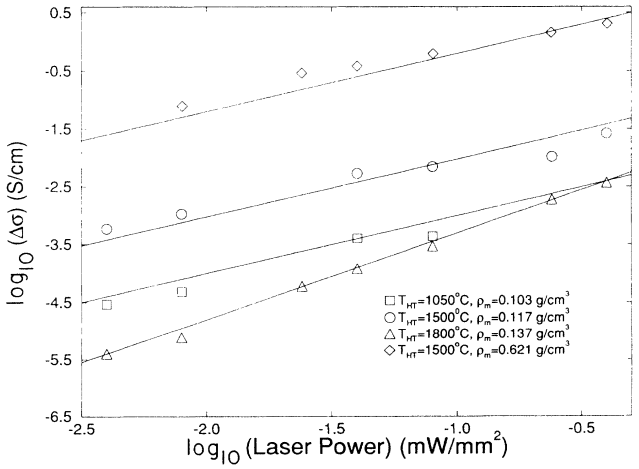

FIG. 5. Log-log plot of photoconductivity measured at 10 K versus laser intensity for carbon aerogel samples with various mass densities ρ_m and heat-treatment temperatures T_{HT}. The data points are compared to solid lines with a slope of 1 for three of the data sets. For the sample with T_{HT} = 1800 ° C and ρ_m=0.137 g/cm^3, the comparison is to a slope of 1.5.

grains (particles) which now become localization sites. It should be noted that this nearest-neighbor hopping behavior is a limiting case of the variable range hopping observed from magnetoresistance data[13] at very low T ($<$10 K).

The log-log plot of photoconductivity versus laser intensity (Fig. 5) shows monomolecular processes for all samples, with the exception of the sample with ρ_m=0.137 g/cm^3 and T_{HT} = 1800 °C. For a monomolecular process, the number of dark carriers significantly exceeds the number of photogenerated carriers.[16] The presence of monomolecular processes at 10 K suggests that the photogenerated carriers are recombining with excess dark carriers, as will be seen later in the $\Delta\sigma/\sigma$ plots.

With these mechanisms in mind for the conductivity and photoconductivity, Fig. 6 illustrates schematically the density-of-states model being considered. Energies are measured as indicated by the arrow in the diagram. Typically, disordered carbon materials tend to be p type, resulting in a Fermi energy, E_F, situated in the valence band. The conduction and valence band mobility edges are denoted by E_C and E_V, respectively. Localized states (shaded regions) exist below E_C and above E_V, while quasicontinuum states exist above E_C and below E_V. The quasicontinuum states result from the spatial confinement introduced by the quantum size of the particles. Free carriers exist between E_F and E_V. The existence of free carriers is evident from the Pauli susceptibility (χ_P) data.[4] With this model, photoexcited carriers can get trapped in localized states above E_V. To account for the long decay times that are observed, screening of the trapped carriers induced by lattice relaxation would have to occur.

To link the above model to the photoconductivity data, we propose a mathematical model to quantitatively explain the observed T dependence of the photoconductivity. As stated earlier, the prominent features of the temperature dependence of the photoconductivity include a maximum in the plots of $\Delta\sigma$ versus temperature. Above and below this maximum, the photoconductivity exhibits an exponential temperature dependence. These similar features have been observed in various chalcogenide glasses such as a-As_2Te_3 and $Ge_{15}Te_{81}Sb_2S_2$.[17–19] The goal of our model is to elucidate the essence of the photoprocesses in carbon aerogels from which we hope to extract important information about the effects of heat treatment on the defect properties of these materials.

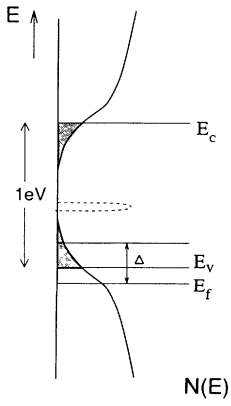

FIG. 6. Schematic diagram showing a physical form of the density of states used to explain the observed photoconductivity data.

To pinpoint the recombination process in our system, a degenerate p-type semiconductor, it is informative to locate the demarcation levels, and from these determine whether the defects present in our system behave as traps or recombination centers for free carriers. In the steady state, the demarcation level for holes, E_{Dp}, is defined as the energy level at which the probability $\bar{n}$ of capturing an excited electron in a trap is equal to the probability of thermally exciting a hole from the same energy level to the valence band, E_V:

$$\bar{n} \equiv n\sigma_n v = e_p \ . \tag{2}$$

Here, σ_n is the capture cross section for electrons, $n = n_0 + \Delta n \simeq \Delta n$ is the electron density in the steady state ($\Delta n \gg n_0$ since E_g is large), n_0 is the electron density in thermal equilibrium, $v = v_n = v_p$ is the electron (hole) velocity, and e_p is the probability for thermal emission of holes from the trapping level. From detailed balance considerations in thermal equilibrium,[20]

$$e_p = v\sigma_p p_0 \exp[-(E_{Dp} - E_F)/kT] \tag{3}$$

for a trap state at the demarcation level E_{Dp} and p_0 is the hole density in thermal equilibrium ($p_0 \gg \Delta p$ in the degenerate semiconductor case). From Eqs. (2) and (3), the demarcation level for holes is given by

$$E_{Dp} - E_F = kT \ln\left(\frac{\sigma_p p_0}{\sigma_n \Delta n}\right) \ . \tag{4}$$

Calculations for the electron demarcation level E_{Dn} give:

$$E_{Dn} - E_F = kT \ln\left(\frac{\sigma_p p_0}{\sigma_n n_0}\right) \ , \tag{5}$$

using $\bar{p} = p_0\sigma_p v$ in thermal equilibrium and $e_n = n_0 v\sigma_n \exp[(E_{Dn} - E_F)/kT]$. In both cases the demarcation level is located at kT's above E_F (since $p_0/\Delta n, p_0/n_0 \gg 1$). Hence, any defect states lying close to the valence band edge act as recombination centers for electrons, and traps for holes; as can be seen later, the defect states in carbon aerogels lie close to E_V. Photoconductivity can then be attributed to the photoholes. Photoelectrons falling into the recombination centers are not likely to get reexcited because of the large band gap and they only recombine when holes fall into the same traps. Recombination is not instantaneous as the electrons are effectively screened by lattice relaxation when they become trapped, thus accounting for the long decay times.

Also, holes excited to traps of the same energy may not necessarily recombine with the trapped electrons, as their spatial locations can be different.

The next step is to find the photoconductivity itself. Consider a single trapping level of density, N_t. The time rate of change of the carrier density in the valence band is given by

$$\frac{dp}{dt} = G - \bar{p}N_t f_t + N_t e_p(1 - f_t) - \beta pn \tag{6}$$

where G is the external generation rate of electron-hole pairs, f_t is the occupancy function of the trapping level, $\bar{p} = (p_0 + \Delta p)\sigma_p v$, and βpn denotes the direct recombination of electrons and holes across the gap. This last term is negligible since most excited electrons become trapped and so do not contribute to direct recombination. A similar equation holds for the conduction electrons:

$$\frac{dn}{dt} = G - \bar{n}N_t(1 - f_t) + N_t e_n f_t - \beta pn \ . \tag{7}$$

The steady-state trap occupancy function f_t can be found by subtracting Eqs. (6) and (7) and applying the steady-state conditions, $dn/dt = 0$ and $dp/dt = 0$. Hence,

$$f_t = \frac{\bar{n} + e_p}{\bar{n} + \bar{p} + e_n + e_p} \ . \tag{8}$$

By taking into account the condition of charge neutrality in the system,

$$\Delta p - \Delta n = N_t \left[\frac{\bar{n} + e_p}{\bar{n} + e_n + \bar{p} + e_p} - \frac{e_p}{e_p + \bar{p}_0} \right] \tag{9}$$

where the right-hand side corresponds to the steady-state trap occupancy minus the thermal equilibrium trap occupancy for electrons. Here, $e_p/(e_p + \bar{p}_0) = 1/\{1 + \exp[(E_t - E_F)/kT]\}$ with $\bar{p}_0 = p_0\sigma_p v$ in thermal equilibrium. Because the hole emission from traps close to E_V is large, and since $p_0 \gg \Delta p$, we can assume $e_p \gg (\Delta p\sigma_p + \Delta n\sigma_n)v$, or equivalently,

$$\frac{\Delta n\sigma_n + \Delta p\sigma_p}{\sigma_p p_0 \exp[-(E_t - E_F)/kT]} \ll 1 \ . \tag{10}$$

Using a Taylor series expansion to the first order on Eq. (10), we obtain

$$\Delta p - \Delta n = N_t \left[\frac{\bar{n}}{\bar{p}_0 + e_p} - \frac{(\bar{n} + e_p)(\Delta n\sigma_n v + \Delta p\sigma_p v)}{(\bar{p}_0 + e_p)^2} \right] . \tag{11}$$

Because most of the photoelectrons become trapped and do not get reexcited to the conduction band, we can consider $\Delta n \ll \Delta p$. Using this assumption and $\bar{n} \ll e_p$ from above, we obtain, after collecting terms in Δp,

$$\Delta p \simeq \frac{(N_t \Delta n\sigma_n/p_0\sigma_p)}{\{1 + (2 + \frac{N_t}{p_0})\exp[-(E_t - E_F)/kT] + \exp[-2(E_t - E_F)/kT]\}} \ . \tag{12}$$

Using the fact that from the dark conductivity, $\mu \propto \exp(-E_A/kT)$ to a good approximation,

$$\Delta\sigma = \Delta pe\mu \propto \frac{N_t e(\Delta n\sigma_n/p_0\sigma_p)\exp(\frac{-E_A}{kT})}{1 + (2 + \frac{N_t}{p_0})\exp(\frac{-(E_t - E_F)}{kT})} \tag{13}$$

$$\propto \frac{A\exp(\frac{-E_A}{kT})}{1 + B\exp(\frac{-\Delta}{kT})} \tag{14}$$

where we ignore the term in $\exp[-2\Delta/kT]$ because it is much less than the $(2 + \frac{N_t}{p_0})\exp(-\Delta/kT)$ term, as is shown in our fits. The solid lines in Fig. 3 are the fit to the experimental data according to Eq. (14). The fitting values of E_A for the photoconductivity (see Table I) are on the same order of magnitude as the activation energies E_a obtained from the dark conductivity data, confirming the self-consistency of the model. Values for B, N_t, and p_0 are listed in Table I for the low density samples. Generally, B increases with T_{HT}, because N_t (obtained from magnetic susceptibility) does not change much with heat treatment.[5] For low values of p_0, the model is still valid as our assumption of $p_0 \gg \Delta p$ holds in the high-temperature regime where the effect of the term in $1/[1 + B\exp(-\Delta/kT)]$ begins to dominate in Eq. (14) and the thermal generation of holes becomes prominent.

So far, we have considered a system consisting of one kind of defect, resulting in a single trapping level in the band gap. If we consider the defect states to be a result of dangling bonds situated near the valence band (dashed region in Fig. 6), then from Table I, the trapping energy, $\Delta \equiv (E_t - E_F)$, is seen generally to decrease with increasing T_{HT} and ρ_m. The decrease in Δ with increasing T_{HT} is due to the system becoming less disordered, effectively pushing E_F closer towards E_V.

If the energy levels associated with the dangling bonds are situated close to midgap, the observed values of Δ are too small to account for the deep position of the dangling bond energies. In that case, we still have justification for using a single energy level. We can go from an exponential distribution of localized states above E_V, as in Fig. 6, to a δ-function-like distribution for the trapping levels in the gap as follows. According to Tiedje and Rose,[21] the density of states, $N(E)$, above E_V is exponential in nature. We can write $N(E)$ in the form of

$$N(E) \propto \exp\{-[E - (E_V + E_p)]/E_W\} \ . \tag{15}$$

The localized states above E_V can be considered as having a characteristic width of energy E_W. As $E_W \to 0$, $N(E) \to E_W\ \delta\{E - (E_V + E_p)\}$. The lowering of the tail state energies by the value E_p is attributed to polaron formation, which is common in disordered systems in which lattice distortions are favored by the presence of vacancies and defects. The energy of the polarons formed in the tail states is given by

$$E_p = \frac{E_1^2}{2Ka^3} \tag{16}$$

where E_1 is the deformation potential, K is the bulk

modulus, and a^3 is the deformation volume.[22] For $(E_V - E_F) \sim 1$ meV (a typical value for disordered carbons) and using $\Delta = E_p + (E_V - E_F)$, for an in-plane deformation potential[23] on the order of 28 eV and an in-plane bulk modulus[24] on the order of 10^{13} dyn/cm^2, the values for Δ listed in Table I would result in lengths on the order of 17 Å for the effective lattice distortion, which is reasonable for the widths of the carbon ribbons being considered. As heat-treatment temperatures and mass density increase, the reduced values of E_p imply larger bulk moduli.

Figure 4 shows that with increasing heat-treatment temperature the ratio $\Delta\sigma/\sigma$ decreases at all temperatures. The low density 1800 °C sample has a very small $\Delta\sigma$, signaling a possible breakdown of our model due to graphitization and hence, a likely emergence of fast recombination processes. There is no maximum in the plot of $\Delta\sigma/\sigma$ versus T, unlike that observed in the plot of $\Delta\sigma$ vs T (Fig. 3). From Eq. (14), and using $\sigma \propto \exp(-E_A/kT)$, it can be seen that $\Delta\sigma/\sigma$ should exhibit a monotonic temperature dependence.

Another feature of carbon aerogels that should be considered is their relation to granular metallic (GM) compounds.[25] Fung *et al.*[13] have classified carbon aerogels and activated carbon fibers (ACF's) as types of GM compounds. Characteristic of these materials is a structure of particles and pores, with free carriers inside the particles. Figure 4 shows that for all samples, the ratio $\Delta\sigma/\sigma$ is less than unity, implying the presence of free carriers even at low T. From Ref. 7, the dc plot of $\Delta\sigma/\sigma$ vs T suggests that there were few free carriers present in the as-prepared samples. However, the ac measurements of $\Delta\sigma$ show a much faster drop in the magnitude of $\Delta\sigma/\sigma$ with increasing T than the dc data (by 2 orders of magnitude). The dc data represent changes in both p and Δp, whereas the ac data, where a gate time shorter than the recombination time is employed, represent changes only in p while Δp is effectively constant. Hence, the ac data really imply that $\Delta\sigma/\sigma < 1$, and hence the presence of free carriers.

For heat-treated samples, especially the highest-density samples, the concentration of trapping levels is reduced. Hence the photoconductivity decreases with increasing heat-treatment temperature, indicating that the carbon aerogels become more graphitic. Evidence of this graphitization with increasing heat-treatment temperature has been observed in TEM micrographs,[26] and is reported elsewhere.

V. CONCLUSIONS

The results presented in this paper suggest that the photoconductivity in carbon aerogels arises from photoholes. The order of magnitude (~10 meV) of $(E_t - E_F)$ obtained from the model suggests that the trapping levels are close to the valence-band mobility edge. The observed long decay times are then a result of screening induced by lattice relaxation when charge carriers are trapped. With increasing T_{HT} and ρ_m, the magnitude of $\Delta\sigma/\sigma$ decreases, suggesting a decrease in the concentration of trapping levels. As the concentration of trapping levels decreases, the system tends to become more graphitic in structure, and hence we observe no measurable photoconductivity in the highest-density sample with T_{HT}=1800 ° C. The photoconductivity parameters in Table I suggest that the low-density heat-treated samples have characteristics similar to the as-prepared sample. The largest difference in parameters is seen between the as-prepared and the heat-treated high-density samples. The functional form for $\sigma(T)$ of the high-density samples is very different from their low-density counterparts. In this sense, the effect of heat treatment is most clearly seen in the samples with higher mass density. This could be due to the ease with which links can be created between grains in the high-density samples under heat treatment. The energies obtained for the thermally activated mobility indicate that nearest-neighbor hopping between grains is an important transport mechanism for carbon aerogels at low temperature.

These measurements show that photoconductivity measurements are highly sensitive to defect states. The photoconductivity data are shown to be sensitive to the whole region of the band gap, whereas conductivity measurements are sensitive to transport between localized states near the Fermi level. Carbon aerogels can be considered as another form of a granular metallic system. The long decay times observed at low temperature (on the order of seconds) need to be studied further. The decay times were previously measured by noting the time for the photocurrent to decay to half its original value. This method makes it difficult to detect fast decay components. Future work should be done to determine the decay time profile in more detail.

ACKNOWLEDGMENTS

We are thankful to Dr. M. Hosoya for assistance and stimulating discussions in the early stages of this work. The MIT authors gratefully acknowledge support from Lawrence Livermore National Laboratory subcontract B130530. The aerogel synthesis was performed under the auspices of the U.S. Department of Energy by Lawrence Livermore National Laboratory under Contract No. W-7405-ENG-48.

[1] For a review, see Mater. Res Bull. **15** (12), 19 (1990).
[2] J. Fricke, Sci. Am. **258**, 92 (1988).
[3] J. Fricke, in *Sol-Gel Science and Technology,* edited by M. A. Aergerter, M. Jafelicci, D. F. Souza, and E. Sanotto (World Scientific, Teaneck, NJ, 1989), p. 482.
[4] A. W. P. Fung, Z. H. Wang, K. Lu, M. S. Dresselhaus, and R. W. Pekala, J. Mater. Res. **8**, 1875 (1993).
[5] J. Chen (private communication).
[6] A. Rose, *Concepts in Photoconductivity and Allied Problems* (Interscience, New York, 1963).

[7] M. Hosoya, G. Reynolds, M. S. Dresselhaus, and R. W. Pekala, J. Mater. Res. **8**, 811 (1993).
[8] K. Kuriyama, M. S. Dresselhaus, and A. W. P. Fung, in *Extended Abstracts of the 20th Biennial Conference on Carbon, Santa Barbara, CA*, edited by Robert Meyer (American Carbon Society, University Park, PA, 1991), p. 300.
[9] K. Kuriyama and M. S. Dresselhaus, J. Mater. Res. **7**, 940 (1992).
[10] T. C. Chieu, M. S. Dresselhaus, and M. Endo, Phys. Rev. B **26**, 5867 (1982).
[11] R. W. Pekala, C. T. Alviso, F. M. Kong, and S. S. Hulsey, J. Non-Cryst. Solids **145**, 90 (1992).
[12] R. W. Pekala, J. Mater. Sci. **24**, 3221 (1989).
[13] A. W. P. Fung, Z. H. Wang, M. S. Dresselhaus, G. Dresselhaus, R. W. Pekala, and M. Endo, Phys. Rev. B (to be published).
[14] J. P. Chausse and J. Hoarau, J. Chim. Phys. **66**, 1062 (1969).
[15] J. Hoarau and G. Volpilhac, Phys. Rev. B **14**, 4045 (1976).
[16] P. Nagels, in *Amorphous Semiconductors*, edited by M. H. Brodsky, Topics in Applied Physics Vol. 36 (Springer-Verlag, Berlin, 1979).
[17] *Photoconductivity and Related Phenomena,* edited by J. Mort and D. M. Pai (North-Holland, Amsterdam, 1976).
[18] T. D. Moustakas and K. Weiser, Phys. Rev. B **12**, 2448 (1975).
[19] T. C. Arnoldussen, R. H. Bube, E. A. Fagen, and S. Holmberg, J. Appl. Phys. **43**, 1798 (1972).
[20] W. Shockley and W. T. Read, Jr., Phys. Rev. **87**, 835 (1952).
[21] T. Tiedje and A. Rose, Solid State Commun. **37**, 48 (1980).
[22] N. F. Mott and E. A. Davis, *Electronic Processes in Non-Crystalline Materials*, 2nd ed. (Clarendon, Oxford, 1979).
[23] S. Ono and K. Sugihara, J. Phys. Soc. Jpn. **21**, 861 (1966).
[24] W. N. Reynolds, *Physical Properties of Graphite* (Elsevier, Amsterdam, 1968).
[25] B. Abeles, P. Sheng, M. D. Coutts, and Y. Arie, Adv. Phys. **24**, 407 (1975).
[26] R. W. Pekala, S. T. Mayer, J. L. Kaschmitter, and F. M. Kong, in Proceedings of the International Symposium on Advances in Sol-Gel Processing and Applications, edited by Yosry A. Attia [Plenum, New York (in press)].